University of Baghdad
College of Engineering
JE
JOURNAL OF ENGINEERING

Mechanical and Energy Engineering

Thermal Performance of Plastic Receiver in Solar Collector

Dr. Kadhim Fadhil Nasir*
Lecturer
Farm Machinery and Equipment Eng. Dept., AL Furat Alawsat Technical University –AL Mussaib
Technical College, Iraq, kka_ff70@yahoo.com

ABSTRACT

A plastic tubes used as absorber of active flat plate solar collector (FPSC) for heating water were studied numerically and experimentally. The set-up is located in Babylon (republic of Iraq) 43.8^0 East longitude and 32.3^0 North latitude with titled of 45^0 toward the south direction. The study involved three dimensions mathematical model for flat coil plastic absorber which solved by FLUENT-ANSYS-R.18 program. Experiments were conducted at outdoor conditions for clear days on January and February 2018 with various water volume flow rates namely (500, 750, 1000, 1250, and 1500 Liter per hour LPH) on each month for Reynolds number range of (1×10^4 to 5×10^4) through the receiver. The experimental results showed improvement in absorber input - output temperature difference, collector efficiency, and water storage temperature; the maximum input - output temperature difference is 3.1 °C, the maximum collector efficiency is 79%, and the maximum water storage temperature is 67 °C. The comparison validates a good agreement between the numerical and experimental results at variable operation conditions with maximum deviation of 4.2%. Also the experimental results were compared with previous study for similar condition and gave a good improvement.

Key words: plastic, absorber, solar collector, water heating, storage temperature, numerical, experimental.

<div dir="rtl">

الاداء الحراري لمستقبل بلاستيكي في مجمع شمسي

د. كاظم فاضل ناصر
قسم هندسة تقنيات المكائن والمعدات الزراعية
جامعة الفرات الاوسط التقنية / الكلية التقنية ـ المسيب

الخلاصة

تم اجراء دراسة عددية وعملية على مجمع شمسي من نوع الصفيحة المستوية الفعال باستخدام انابيب بلاستيكية كمستقبل شمسي. اجريت الدراسة العملية في محافظة بابل (العراق) عند خط طول 43.8 درجة شرقا و خط عرض 32.3 درجة شمالا مع زاوية ميلان 45 درجة مع الافق باتجاه الجنوب. تضمنت الدراسة بناء نموذج رياضي ثلاثي الابعاد للمستقبل البلاستيكي وتم حله بواسطة برنامج الانسز فلونت 18 . تم اجراء التجارب العملية في الاجواء الخارجية خلال شهري كانون الثاني وشباط 2018 لمعدلات جريان مختلفة للماء المار داخل المستقبل وهي (500, 750, 1000, 1250,و 1500) لتر بالساعه خلال كل شهر ولمدى رقم رينولد من

</div>

10*4‏1 الى 5*10‏4. اثبتت النتائج العملية فاعلية في فرق درجات الحرارة للماء مابين الدخول والخروج للمستقبل وفاعلية في كفاءة المجمع الشمسي ودرجات حرارة الماء المخزون حيث كان اكبر فرق بدرجات الحرارة هو 3,1 درجة مئوية و اكبر كفاءة للمجمع الشمسي هي 79% واعلى درجة حرارة للماء المخزون هي 67 درجة مئوية. تم اجراء مقارنه مابين النتائج العددية والعملية لهذا البحث وكان التطابق جيدا مع وجود فرق مقداره 4,2% كما تم اجراء مقارنه ما بين النتائج العملية لهذه الدراسة ونتائج الدراسات السابقة عند ظروف تشغيل متشابهة واعطت المقارنة افضلية جيده للدراسة الحالية.

الكلمات الرئيسية: بلاستك, مستقبل, مجمع شمسي, تسخين الماء, درجة حرارة الخزن, عدديا, عمليا.

1. INTRODUCTION

Flat plate solar collectors are commonly designed for applications of 40 and 60°C in case of hot water systems. Copper is the standard tubing material used in solar water heaters. The requirement to other materials with a lesser cost is necessary for construction **Schweiger, 1997**. Solar collectors are special type of heat exchangers which convert solar energy to internal energy in medium. The collected solar energy was approved from a circulating fluid directly to heating water or space or by storage tank then drawn for users at cloudy days and night **Kalogirou, 2004**. Solar radiation represented clean form of useful energy, which almost needed all natural processes on earth **Assilzadeha, et al., 2005**. Polymeric materials are employed in thermal solar applications via replaced single parts by polymers **Christoph, 2014.** Fossil energy represented energy source and limited in quantity. The limited resources of fossil energy lead to reason for needed of renewable energies growth. Renewable energies derived from renewable and natural **Bridle, et al., 2014** and **Ramelan, et al., 2016**.

Bansal, et al.,1983 studied the performance of solar air heating collector which includes porous fabric absorber putting between two PVC foils. The results shown a temperature increase of 17 °C for solar energy of 690 W/m² with air flow rate of 800 m³/h and efficiency reached to 71 percent. **Schmidt** and **Goetzberger, 1990** suggested employed insulation to decrease the energy losses from the absorber thus the insulating material put over the absorber surface. The effect of using single and double glazing cover with vacuum tubes and absorber are studied by **Mason** and **Davidson, 1995**. **Bartelsen, et al., 1999** investigated the using of elastomer metal absorbers for employed in roofs. The metal plates for absorbers have integrated clip profiles. The major advantages of the absorber are the inherent freeze resistance without adding antifreeze additives. Also it represented resistance against the corrosion. **Brunold,** and **Kunststoffkollektoren, 2010** studied the polymer collector and the effective of cost. The results show the maximum temperatures are high for the suggested polymeric materials and cost reducing. Thermal solar systems were investigated by **Kaiser, et al., 2012** by simulation collector employed polymeric materials. The analysis of collector included design with glazing twin wall sheet. The consequences of system simulation were compared with conventional system for estimating the effect on the part temperatures and system efficiency. **Luis**, and **Nicolás, 2013** studied the using of plastic hose which connected in series in solar collector. The advantage of plastic tubing for improving a simple construction collector is prices; about 70 dollars for a unit. It reached good thermal performance. The effects of using a plastic cylindrical absorber in solar air heating system with back isolation and double covers for heating and drying processes are investigated by **Abdullah and Bassiouny, 2014** experimentally and theoretically. The maximum output temperature was achieved at the lowest air mass flow rate. The maximum value was 81° C for 0.13 kg/s mass flow rate. **Al-Douri and Abed,**

2016 investigated the overviews of the potential future difficulties and promising supply of the solar energy in Iraq. A study of the radiation energy levels was accompanied. **Kadhim, 2017** studied the effect of using copper flat coil tube as receiver in flat plate solar collector numerically and experimentally in Iraq. The results show a maximum storage temperature of water is 71 °C and maximum collector efficiency is 81%.

The present study includes first the thermal analyses of FPSC performance, while the second presents the numerical analysis of the developed mathematical model for the flat coil plastic receiver, and then presents the experimental setup. Finally, the validations between the experimental and numerical results are presented. The aim of this investigation is evaluating the performance of the solar water collector with plastic absorber in the climatic conditions of Iraq during the winter.

2. THERMAL PERFORMANCE OF FPSC

The thermal efficiency represented the main solar collector performance **Pati and Deshmukh, 2015**. The energy losses of solar collector are the effect of convection heat transfer and radiation that transferred between the absorber tubes and the collector glass cover. The overall heat loss coefficient (U_L) considered as **Li** and **wang, 2006**.

$$U_L = \left[\frac{A_r}{A_g\left(h_{c.g-a} + h_{r,g-a}\right)} + \frac{1}{h_{r,r-g}}\right]^{-1} \tag{1}$$

Where: $h_{c,g-a} = h_w = \dfrac{Nu_a k_a}{D_g}$ $\tag{2}$

Nusselt number (Nu_w) of water estimated as **Li** and **wang, 2006**:

$$Nu_w = 0.4 \times 0.54 \times Re_a{}^{0.53} \text{ for } 0.1 < Re_a < 1000 \tag{3}$$

$$Nu_w = 0.3 \times Re_a{}^{0.53} \text{ for } 1000 < Re_a < 50000 \tag{4}$$

Reynolds number (Re_w) of water flow inside absorber is considered as **Jacobson, et al., 2006**:

$$R_{ea} = \frac{\rho_a v_a D_g}{\mu_a} \tag{5}$$

$$h_{r,g-a} = \varepsilon_g \delta\left(T_g + T_a\right)\left(T_g^2 + T_a^2\right) \tag{6}$$

$$h_{r,r-g} = \frac{\delta\left(T_r + T_g\right)\left(T_r^2 + T_g^2\right)}{\frac{1}{\varepsilon_r} + \frac{A_r}{A_g}\left(\frac{1}{\varepsilon_g} - 1\right)} \tag{7}$$

The overall heat transfer coefficient (U_o) is the heat transfer coefficient for the fluid which based on the absorber outer diameter ($D_{r,o}$) as **Jacobson, et al., 2006**:

$$U_o = \left[\frac{1}{U_L} + \frac{D_{r,o}}{h_f D_{r,i}} + \frac{D_{r,o} ln\left(\frac{D_{r,o}}{D_{r,i}}\right)}{2k}\right]^{-1} \tag{8}$$

Collector efficiency factor (F') is the ratio of actual useful energy and useful energy collected **Jacobson, et al., 2006**:

$$F' = \frac{1/U_L}{\frac{1}{U_L} + \frac{D_{r,o}}{h_f D_{r,i}} + \frac{D_{r,o}ln\left(\frac{D_{r,o}}{D_{r,i}}\right)}{2k}} \qquad (9)$$

The heat removal factor or correction factor, F_R, is the ratio of the actual gained useful energy to that gained if the absorber surface is at the collector input fluid temperature which considered as **Jacobson, et al., 2006**:

$$F_R = \frac{m_f C_p}{A_r U_L}\left[1 - exp\left(-\frac{A_r U_L F'}{m_f C_p}\right)\right] \qquad (10)$$

The useful solar energy that reached as heat (Q_u) achieved to the absorber as **Ma, et al., 2011**:

$$Q_u = mc_p(T_0 - T_i) \qquad (11)$$

Where: T_i and T_o are mean the input and output temperatures of water, respectively.

The immediate thermal collector efficiency η_{th} is the ratio of heat reaching (Q_u) providing to area of aperture A_a and intensity of radiation (I) which is full on the collector **Ma, et al., 2011**.

$$\eta_{th} = \frac{mc_p(T_0 - T_i)}{I\,A_a} \qquad (12)$$

The properties of water that used are temperature dependent which derived from water properties tables as:

$K = 0.00000002T^3 - 0.00001T^2 + 0.0023T + 0.5568$

$\mu = -0.000002T^3 + 0.0005T^2 - 0.0428T + 1.6944$

$\rho = 0.00001\,T^3 - 0.0056\,T^2 + 0.0037T + 1000.3$

$C_p = 0.0000001\,T^3 + 0.00003\,T^2 - 0.0017T + 4.2084$

3. N UMERICAL ANALYSIS
The numerical analysis includes make a three dimensional system (r, θ, z) mathematical model as shown in **Fig.1**, and mesh construction is shown in **Fig.2**. Descried model domain with mesh dimensions as shown in **Table 1**, applying the boundary conditions for solution governing equations of continuity, momentum, and energy for turbulence steady state are done by ANSYS FLUENT-18. The assumptions considered in the present study include: The receiver is simulated under steady state conditions, the working fluid is Newtonian and incompressible fluid, three dimensional polar coordinates models are considered, no heat Source, and constant wall heat flux and constant water properties as shown in **Table 2**.
Continuity equation **Bird, et al., 1987**

$$\frac{1}{r}\frac{\partial(\rho r v_r)}{\partial r} + \frac{1}{r}\frac{\partial(\rho v_\theta)}{\partial \theta} + \frac{\partial(\rho v_z)}{\partial z} = 0 \tag{13}$$

Momentum equation **Bird, et al., 1987**

r-

$$v_r\frac{\partial v_r}{\partial r} + \frac{v_\theta}{r}\frac{\partial v_r}{\partial \theta} + v_z\frac{\partial v_r}{\partial r} - \frac{v_\theta^2}{r} = -\frac{1}{\rho}\frac{\partial p}{\partial r} + \frac{\mu}{\rho}(\frac{1}{r}\frac{\partial}{\partial r}\left(r\frac{\partial v_r}{\partial r}\right) + \frac{1}{r^2}\frac{\partial^2 v_r}{\partial \theta^2} + \frac{\partial^2 v_r}{\partial z^2}\frac{v_r}{r^2} -$$
$$\frac{2}{r^2}\frac{\partial v_\theta}{\partial \theta}) \tag{14}$$

θ-

$$v_r\frac{\partial v_\theta}{\partial r} + \frac{v_\theta}{r}\frac{\partial v_\theta}{\partial \theta} + v_z\frac{\partial v_\theta}{\partial r} + \frac{v_r v_\theta}{r} = -\frac{1}{\rho}\frac{\partial p}{\partial \theta} + \frac{\mu}{\rho}(\frac{1}{r}\frac{\partial}{\partial r}\left(r\frac{\partial v_\theta}{\partial r}\right) + \frac{1}{r^2}\frac{\partial^2 v_\theta}{\partial \theta^2} +$$
$$\frac{\partial^2 v_\theta}{\partial z^2} - \frac{v_\theta}{r^2} + \frac{2}{r^2}\frac{\partial v_r}{\partial \theta}) \tag{15}$$

z-

$$v_r\frac{\partial v_z}{\partial r} + \frac{v_\theta}{r}\frac{\partial v_z}{\partial \theta} + v_z\frac{\partial v_z}{\partial z} = -\frac{1}{\rho}\frac{\partial p}{\partial z} + \frac{\mu}{\rho}(\frac{1}{r}\frac{\partial}{\partial r}\left(r\frac{\partial v_z}{\partial r}\right) + \frac{1}{r^2}\frac{\partial^2 v_z}{\partial \theta^2} + \frac{\partial^2 v_z}{\partial z^2}) \tag{16}$$

Energy equation **Bird, et al., 1987**

$$\rho c_p(v_r\frac{\partial T}{\partial r} + \frac{v_\theta}{r}\frac{\partial T}{\partial \theta} + v_z\frac{\partial T}{\partial z}) = k\left(\frac{\partial^2 T}{\partial r^2} + \frac{1}{r}\frac{\partial T}{\partial r} + \frac{1}{r^2}\frac{\partial^2 T}{\partial \theta^2} + \frac{\partial^2 T}{\partial z^2}\right) \tag{17}$$

Turbulence model Reynolds-Averaged Navier-Stokes (RANS) equations in tensor notation are given by (the over bar on the mean velocity has been dropped)**.**

$$\frac{\partial \rho}{\partial t} + \frac{\partial \rho U_i}{\partial x_i} = O \tag{18}$$

$$\frac{\partial_i}{\partial t}(\rho u_i) + \frac{\partial u}{\partial x_j}(\rho u_i u_j) = -\frac{\partial P}{\partial x_i} + \frac{\partial}{\partial x_i}\left[\mu\left(\frac{\partial u_i}{\partial x_j} + \frac{\partial u_j}{\partial x_i} - \frac{2}{3}\delta_{ij}\frac{\partial u_i}{\partial x_i}\right)\right] + \frac{\partial}{\partial x_j}\left(\overline{\rho u_i' u'_j}\right) \tag{19}$$

The two equation turbulence models solve two transport equations to represent the turbulent properties and get the eddy viscosity. This allows the model to account for history effects like convection and diffusion of the turbulent energy. The transported variables are the turbulent kinetic energy K and the specific dissipation ε for K-ε model. The first transport variable determines the energy in turbulence while the second variable determines the scale of the turbulence it defined as **Bhaskaran, 2013**:

$$\frac{\partial(\rho k)}{\partial t} + \frac{\partial}{\partial xj}(\rho Uj k) = \frac{\partial}{\partial xj}\left[\left(\mu + \frac{\mu_t}{\sigma_k}\right)\frac{\partial k}{\partial xj}\right] + P_k - \rho\varepsilon + P_{kb} \tag{20}$$

$$\frac{\partial(\rho\varepsilon)}{\partial t} + \frac{\partial}{\partial xj}(\rho Uj\varepsilon) = \frac{\partial}{\partial xj}\left[\left(\mu + \frac{\mu_t}{\sigma_\varepsilon}\right)\frac{\partial\varepsilon}{\partial xj}\right] + \frac{\varepsilon}{k}(c_{\varepsilon 1}P_k - c_{\varepsilon 2}\rho\varepsilon + c_{\varepsilon 3}P_{\varepsilon b}) \tag{21}$$

Where $C_{\varepsilon 1} = 1.44$, $C_{\varepsilon 2} = 1.92$ and $\sigma_k = 1$

And P_{kb} and $P_{\varepsilon b}$ represent the influence of the buoyancy forces. P_k is the turbulence production due to viscous forces, which modeled using:

$$P_k = \mu_t \left(\frac{\partial U_i}{\partial x_j} + \frac{\partial U_j}{\partial x_i} \right) \frac{\partial U_i}{\partial x_j} - \frac{2}{3} \frac{\partial U_k}{\partial x_k} \left(3\mu_t \frac{\partial U_k}{\partial x_k} + \rho k \right) \tag{22}$$

The K-ε model assumes that the turbulence viscosity is linked to the turbulence kinetic energy and dissipation via the relation **Bhaskaran, 2013**:

$$\mu_t = C_\mu \rho \frac{k^2}{\varepsilon} \tag{23}$$

Where $C_\mu =0.09$

There are mainly two types of approaches in volume meshing, structured and unstructured meshing. A structured grid was used in the present model. The convergence criterion was satisfied when the absolute differences between two following iterations are less than 10^{-6}. To ensure grid-independent solutions, a number of non-uniform grids were exposed for testing procedure. The grid node concentrations of 212340, 432572, and 505116 have been tested and the results of these cases were compared with the experimental results. The effect of the number of mesh nodes on the temperature difference of water for flat coiled absorber is shown in **Fig.3**. It can be shown that the nearest numerical solution for the experimental is that of the 505116 node.

Table 1. Best model specifications**.**

Dimension	Value	Unit
Node	506116	-
Element	1662831	-
Cell minimum size	4.4989×10^{-4}	m
Cell maximum size	8.9979×10^{-2}	m
Face maximum size	4.4989×10^{-2}	m

Table 2. Boundary conditions of model**s.**

Parameter	Value	Unit
Heat flux rate	1122 (for all flow rates)	W/m^2
Inlet velocity for each flow rate		m/s
500 LPM		
750 LPM	1.13	
1000 LPM	1.69	

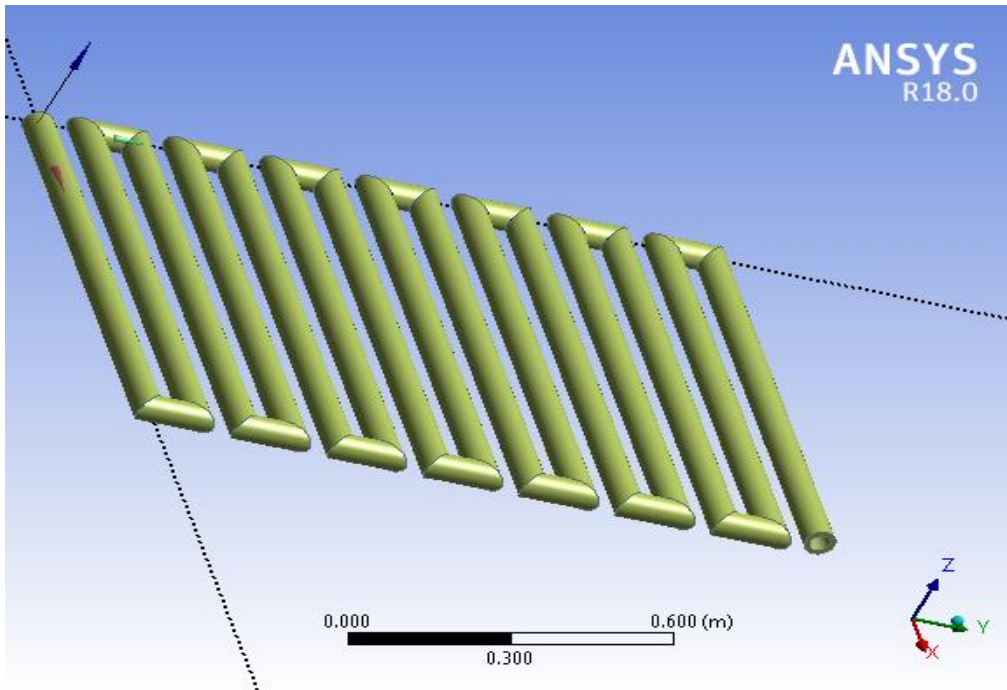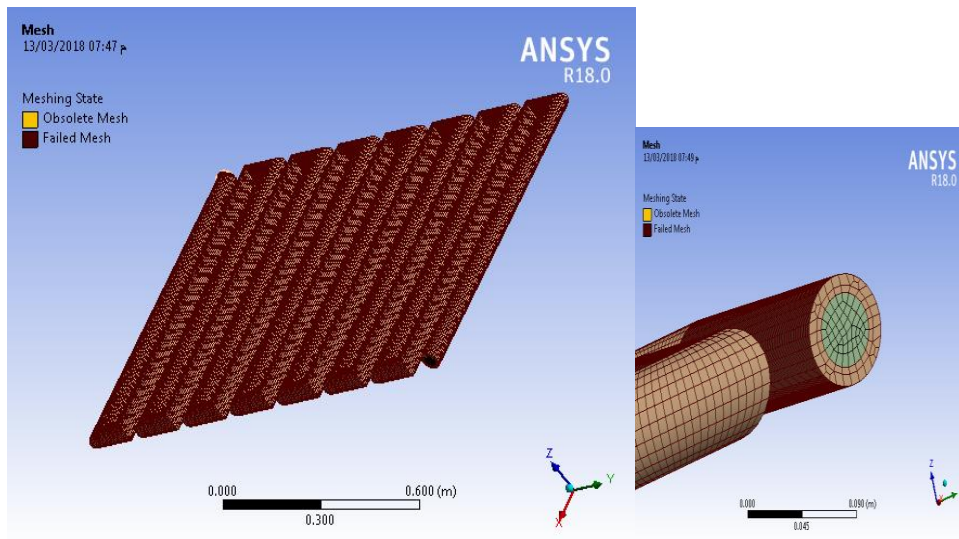| 1250 LPM 1500 LPM	2.26 2.83 3.39	
Inlet temperature	327 (for all flow rates)	K
Density	998.2	Kg/m^3
Specific heat	4182	J/kg.K
Thermal conductivity	0.6	W/m.K
Viscosity	0.000512	Kg/m.s

Figure 1. Mathematical model**.**

Figure 2. Mesh structure of the mathematical model.
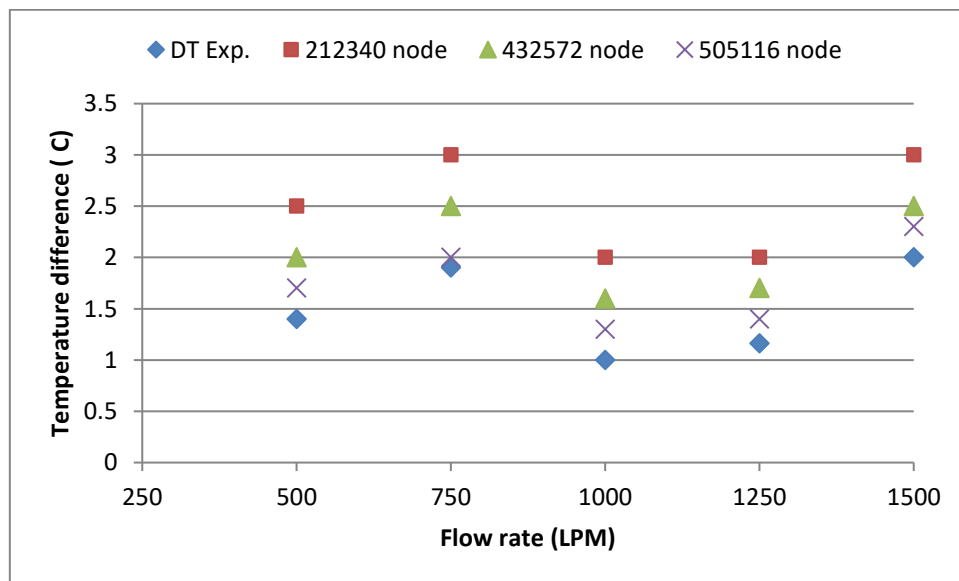
Figure 3. Grid independent test**.**

4. EXPERIMENTAL SETUP

A plastic absorber has a flat coil form in flat plate solar water collector is employed in the current investigation. The specification of the present collector displayed in **Table 3**. This experimental setup was done in Iraq- Babylon, that placed at 43.8^0 East longitude and $32^0 3'$ North latitude with titled of 45^0. The tests occurred outdoor on January and February 2018. The Experimental setup system and its diagram are presented in **Fig.4** and **Fig.5**. The plastic absorber outer surface was painted by black paint. The space between the plastic absorber and glass is 30 mm. Active system was considered with AC water pump and insolation with 50 mm thickness of glass wool were used. Variable water discharges are used namely of (500, 750, 1000, 1250, and

1500) liter per minute (LPM) with Reynolds number range of (1×10^4 to 5×10^4) that characterized turbulent flow through the receiver for 5 clear day on each month for January and February 2018 as shown in **Table 4**.

Table 3. FPSC specifications**.**

consideration	Amount
Area of collector	2.4 m^2
Width of collector	2.4 m
Length of collector	1 m
Length of absorber	17.4 m
Turn number	7.5
Thickness of tube wall	4.2 mm
Inner diameter of absorber	12.52 mm
Single-glass cover thickness	3.5 mm
Orientation	Fixed direction

Table 4. Experimental tests dates.

Volume flow rate	January 2018	February 2018
500	27/1/2018	4/2/2018
750	28/1/2018	5/2/2018
1000	29/1/2018	6/2/2018
1250	30/1/2018	7/2/2018
1500	31/1/2018	8/2/2018

Figure 4. The experimental setup.
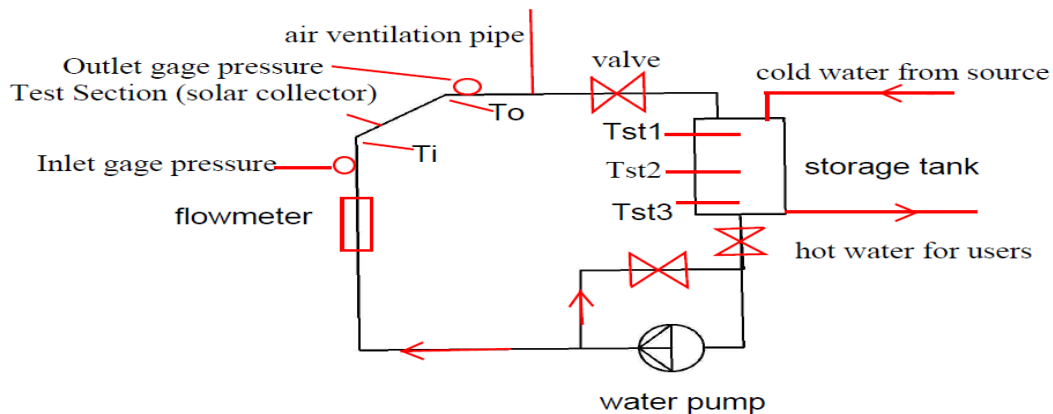
Figure 5. The experimental diagram.

5. MEASUREMEMTS

The measurements include ambient temperature (T_a), input temperature (Ti) and the output temperature (To), Absorber wall temperatures, solar intensity (I), water discharge, wind speed. All measurements are done each half hour. Thermocouples types (K) with diameter of 0.1 mm are employed for measuring temperatures with digital data logger as displayed in **Fig.6**. Pyranometer CMP22 model with data logger are used for measuring solar intensity as shown in **Fig.7**. Lutran anemometer used to measure the wind speed as displayed in **Fig.8**.

Figure 6. Digital data logger.

Figure 7. Pyranometer CMP22 model.

Figure 8. Lutran anemometer.

6. RESULTS

The results obtained from this study include presentation of numerical solution results and experimental results, then shows the comparison between them and indicate the error analysis.

6.1 Numerical results

The numerical solution for the mathematical model involves analysis of five flow rates namely (500, 750, 1000, 1250, and 1500 liter per hour) and sixteenth runs for each water flow rate to estimate the output temperature of the absorber numerically for the same boundary conditions of experiments. **Fig.9, Fig.10, and Fig.11** show samples of the water temperature contours inside the absorber in the case of 750, 1000, and 1250 LPM. It can be clear that the distribution of temperature is increased along the absorber and near the outer wall. Also, it can be shown that the water

temperature difference is reduced with increasing of water volume flow rate. **Fig.12, Fig.13, and Fig.14** show samples of pressure drop contours inside the absorber in the case of 750, 1000, and 1250 LPM. It can be see that the pressure is decreased along the absorber due to restriction against water flow. It can be shown that the pressure drop is increased with increasing of water volume flow rate.
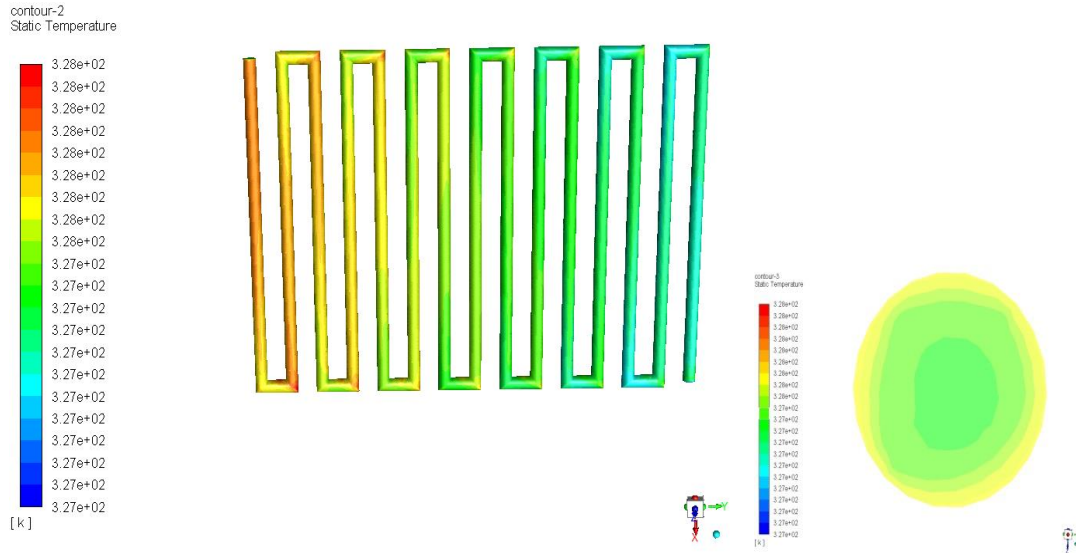
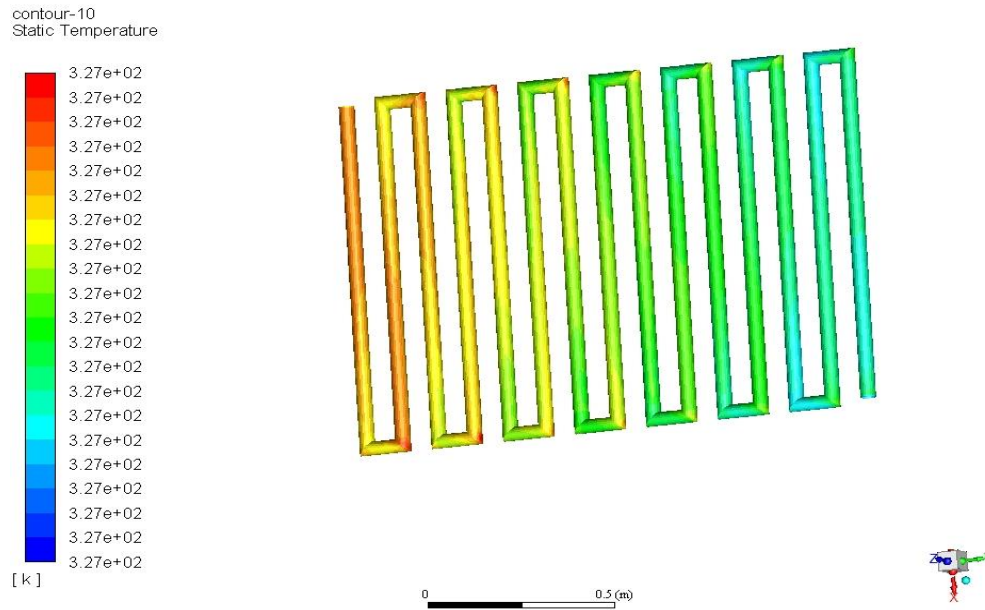**Figure 9.** Temperature contour for 750 LPM.
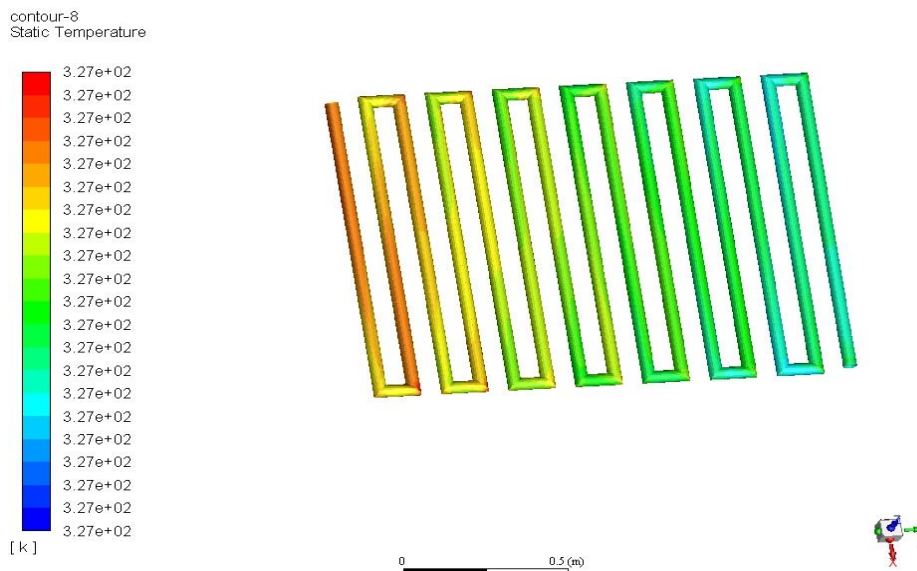
Figure 10. Temperature contour for 1000 LPM.
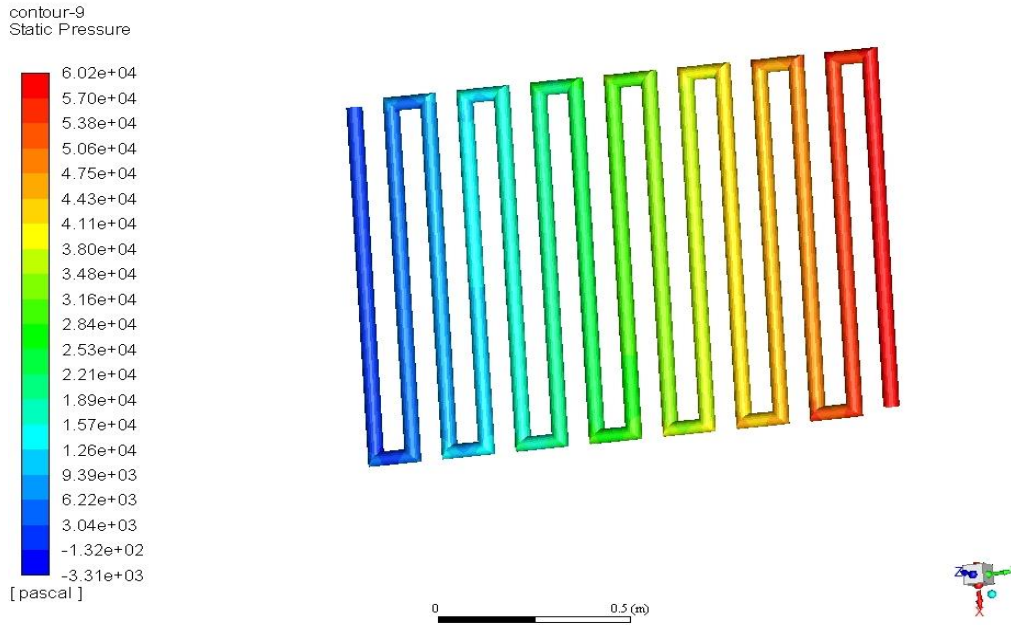
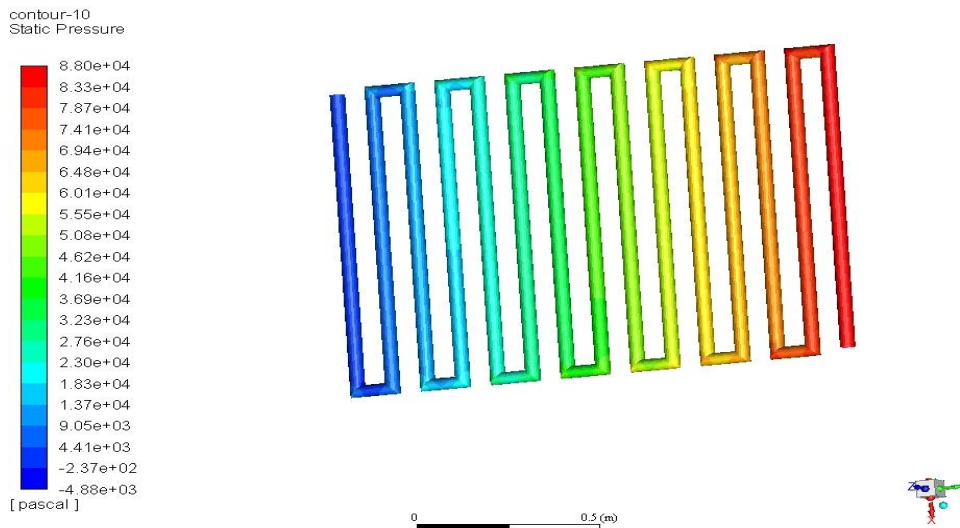**Figure 11.** Temperature contour for 1250 LPM
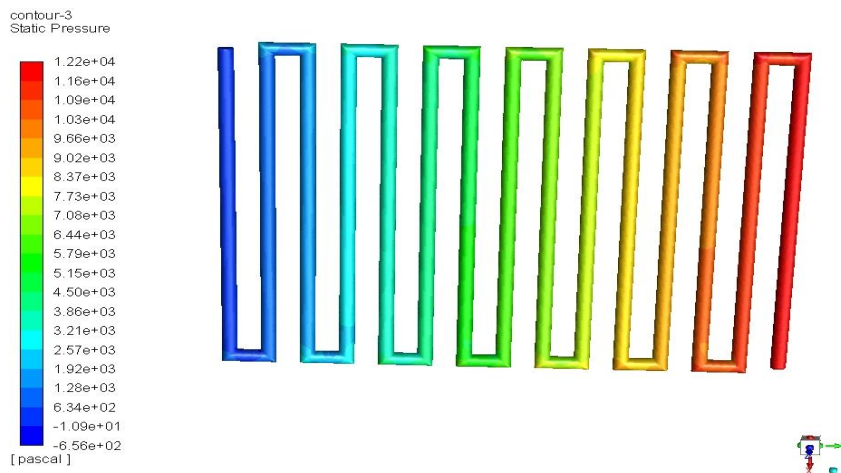
Figure 12. Pressure contour for 750 LPM.

49

Figure 13. Pressure contour for 1000 LPM.

Figure 14. Pressure contour for 1250 LPM.

6.2 Experimental results

Fig.15 shows a sample of the description for input, output, ambient temperatures and solar intensity along the hourly clear day. It clear that the differences between the ambient temperature and input-output temperatures are increased with hourly time due to the absorbing of solar energy by the plastic material absorber tube then transferred to the water which flows inside the absorber tube. Also, the solar intensity

that falls on the collector began increased on the early time till the noon then decreased continuously till the evening.
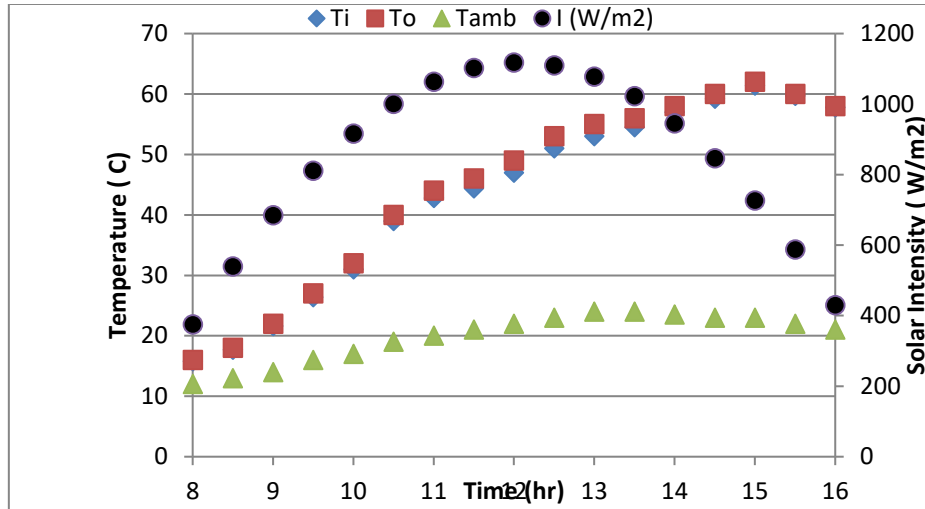
Figure 15. Input, output, ambient temperatures, and solar intensity.

Fig.16 and **Fig.17** show the water input – output temperature difference through the absorber on January and February 2018. It can be seen that the maximum temperature difference occurs at the noon due to increasing in the solar intensity; the maximum temperature difference on January 2018 is 2.7 °C at 12:30 pm for 500 LPH, while the maximum temperature difference on February 2018 is 3.1 °C at 12:30 pm for 1250 LPH.
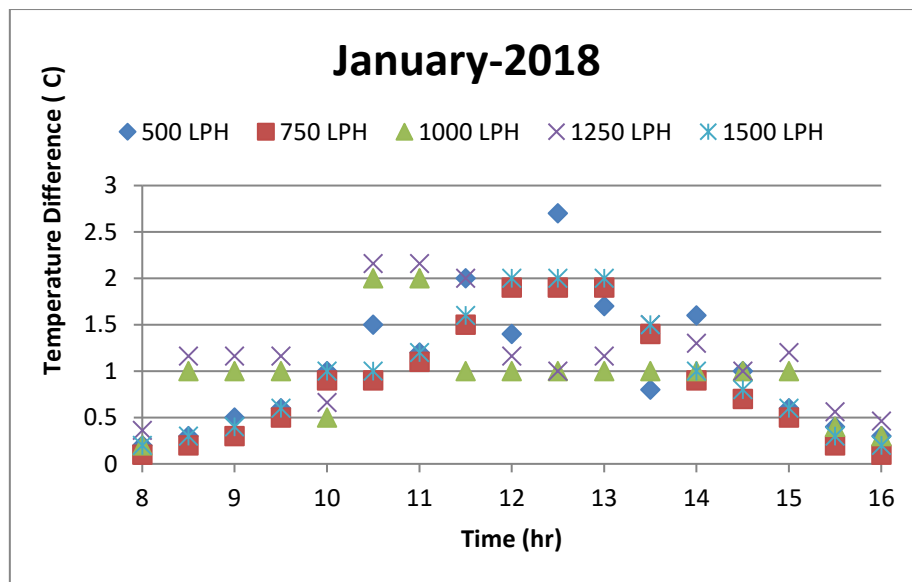
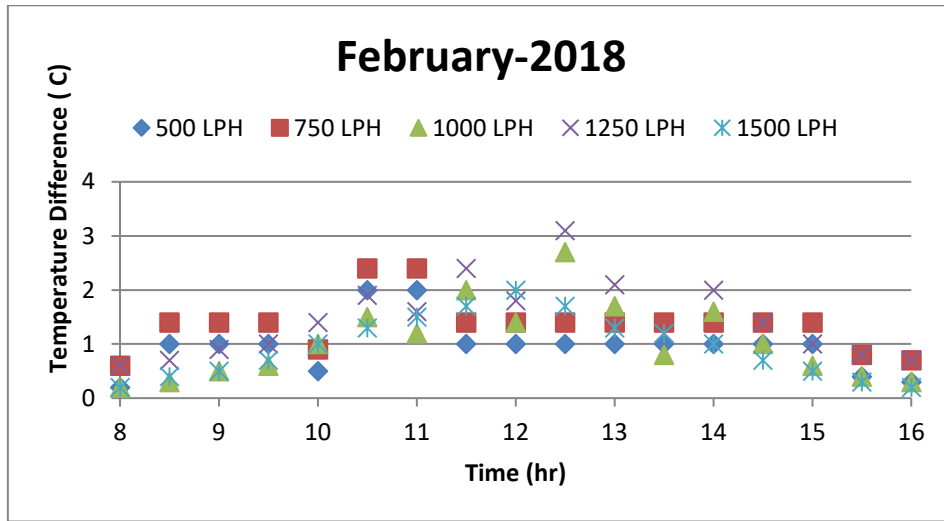**Figure 16.** Input – Output temperature difference on Jan. 2018.

Figure 17. Input – Output temperature difference on Feb. 2018.

Fig.18 and **Fig. 19** show the collector efficiency that estimated along the hourly day time. It be seen that the collector efficiency ranged from 10% to 64% and the maximum efficiency occurs at 13:00 pm for volume water flow rate of 1500 LPH on January 2018 due to increasing in the solar intensity, while it ranged from 12.1% to 79% the maximum efficiency occurs at 12:30 pm for volume water flow rate of 1250 LPH on February 2018.
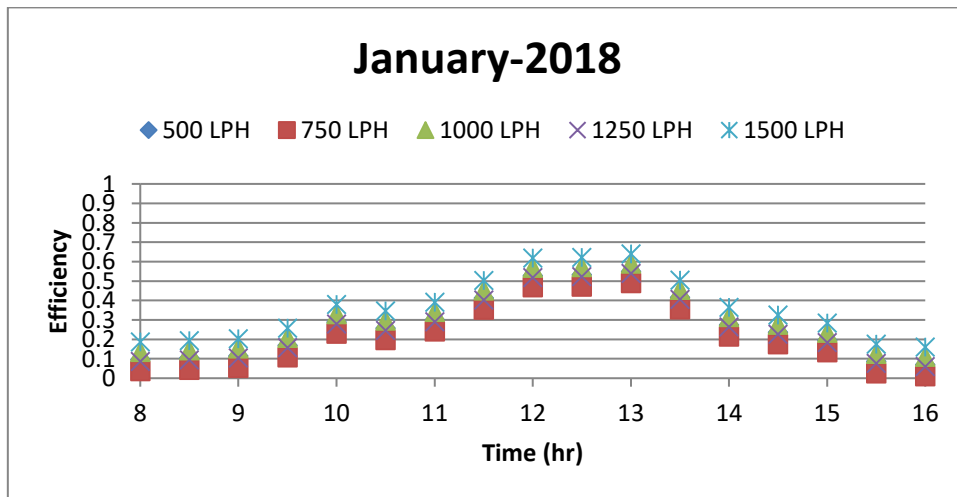

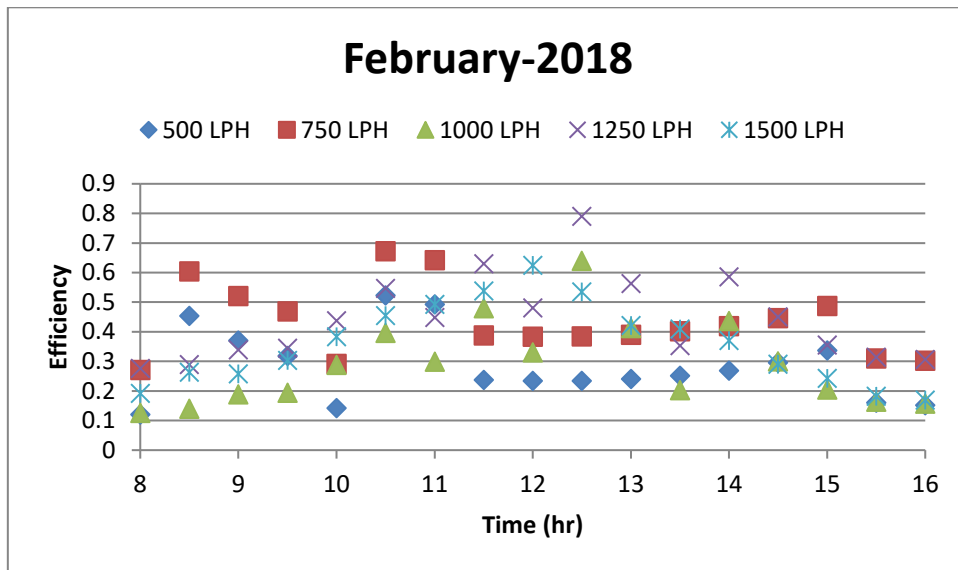**Figure 18.** Collector efficiency on Jan. 2018.

Figure 19. Collector efficiency on Feb. 2018.

Fig.20 and **Fig. 21** show the water storage temperature that measured along the hourly day time. It be seen that the maximum water storage temperature is 65 °C which occurs at 16:00 pm for volume water flow rate of 1250 LPH on January 2018, while the water storage temperature is 67 °C which occurs at 16:00 pm for volume water flow rate of 1250 LPH on February 2018, that's occurred due to increasing in the solar intensity along the test days.
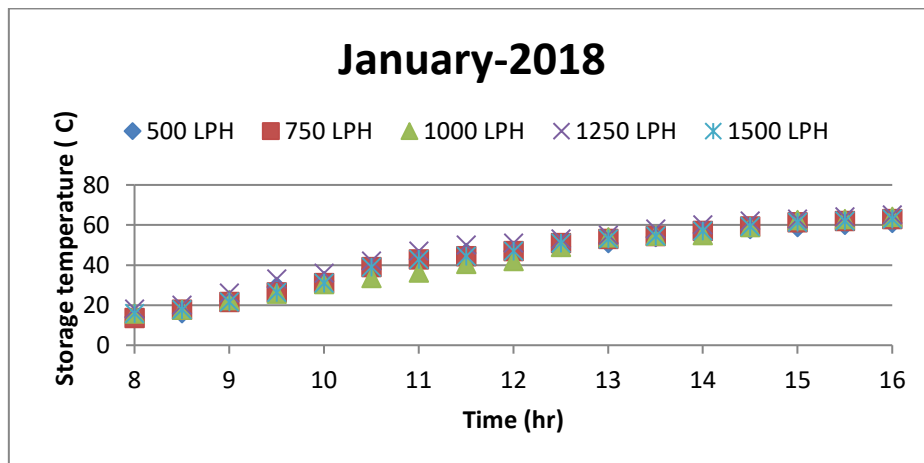

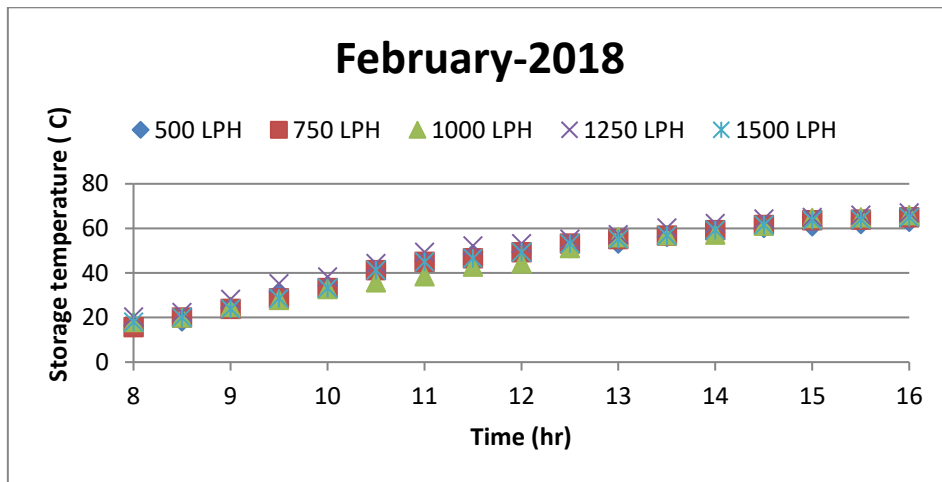**Figure 20.** Storage water temperature on Jan. 2018.

February-2018

◆ 500 LPH ■ 750 LPH ▲ 1000 LPH ✕ 1250 LPH ✱ 1500 LPH

Figure 21. Storage water temperature on Feb. 2018.

Fig.22 and **Fig. 23** show the calculating thermal instantaneous efficiency with great values of incident solar energy, input temperature of water in absorber, and ambient temperature for a period test time of 10:30 am to 14:30 pm **Duffie** and **William, 2013**. The thermal instantaneous efficiency correlated with (Ti-Ta)/I values linearly as:

For January 2018

$$\eta_{th} = 0.611 - 6.6985 \left(\frac{Ti - Ta)}{I} \right) \qquad (24)$$

While for February 2018

$$\eta_{th} = 0.5927 - 7.6113 \left(\frac{Ti - Ta)}{I} \right) \qquad (25)$$

The collector efficiency is plotted against (Ti – Ta)/I. The slope of this line (- F$_R$ U$_L$) represents the rate of heat loss from the collector.
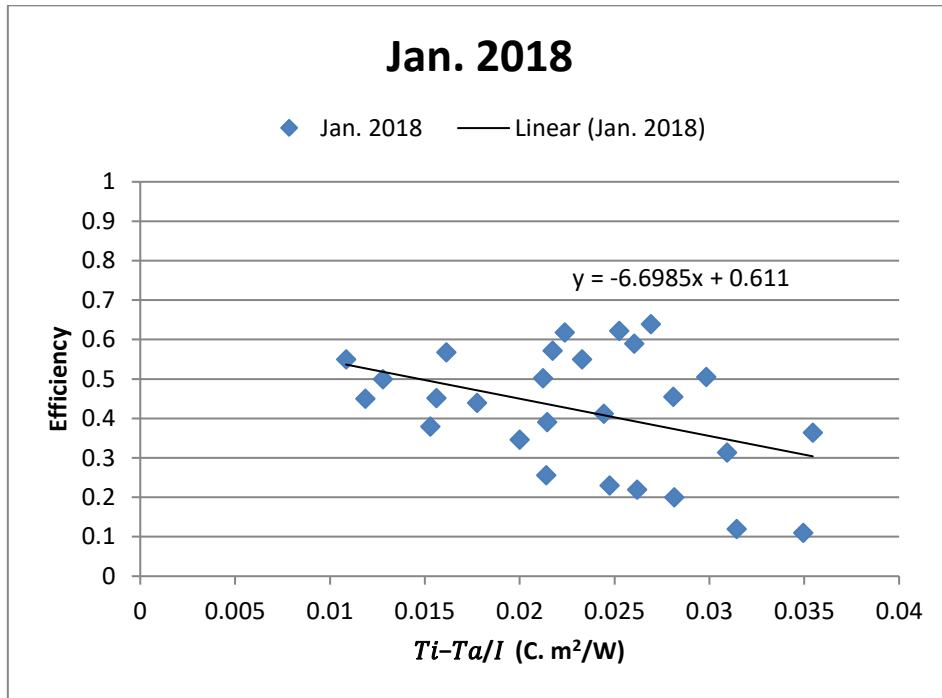
Figure 22. Collector operation on Jan. 2018.

Figure 23. Collector operation on Feb. 2018.

Fig.24 presented the output temperature of water between the numerical and experimental with hourly time. The numerical analysis involved employed specified boundary conditions as inlet temperature and constant heat flux value for each hour. It seen that the small variation in output temperature. The deviation between the numerical and experimental output temperature is 4.2%.

55

1500 LPh -Jan. 2018
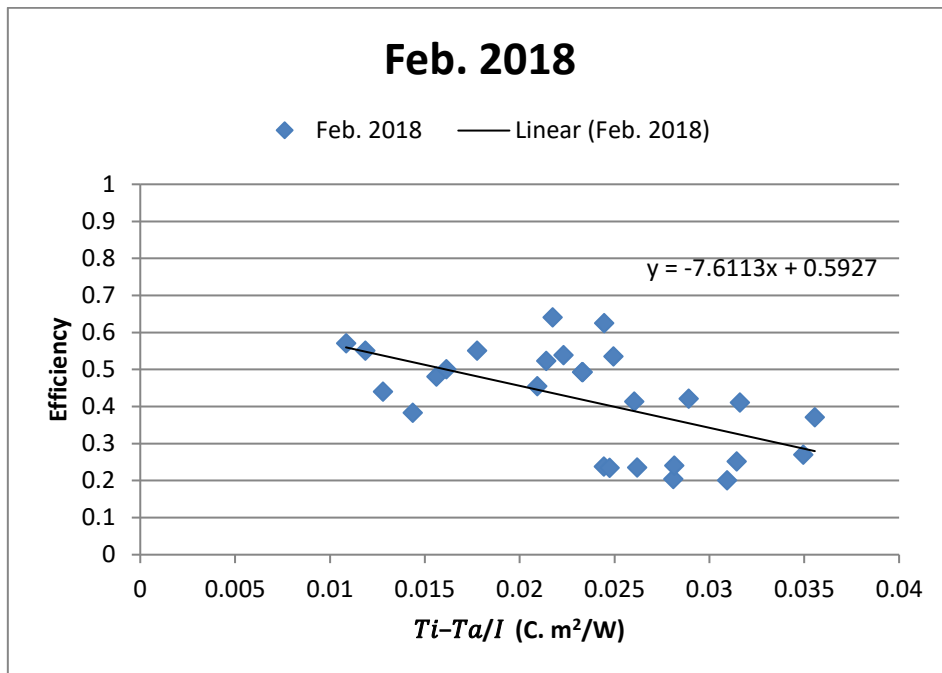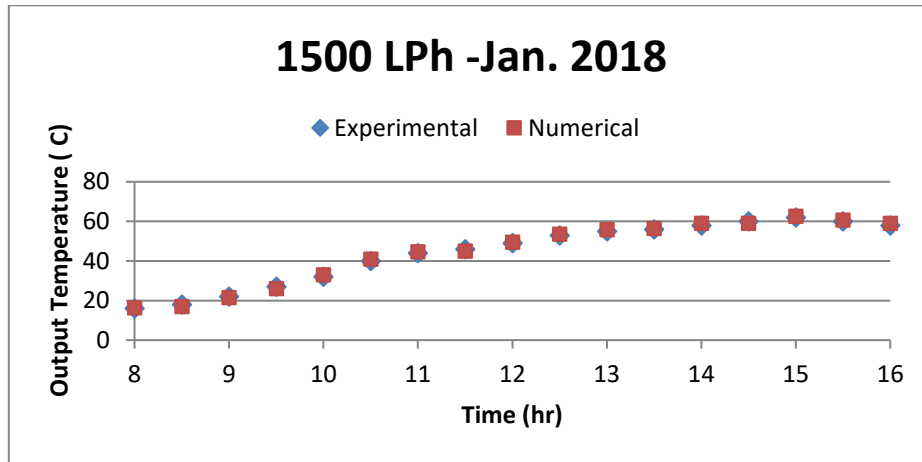
◆ Experimental   ■ Numerical

Figure 24. Output temperature comparison between numerical and experimental.

Fig. 25 Shows the transient variation of absorber input-output temperature. It displays temperature drop due to sudden reduction of the solar radiation on the collector to zero. This type of collector testing is the determination of the heat capacity of a collector in terms of a time constant at which the following equation is reached **Duffie** and **William, 2013**:

$$\frac{T_{o,t}-T_i}{T_{o,init}-T_i} = 0.368 \tag{26}$$

where:

$T_{o,t}$ is the water outlet temperature at time t , $T_{o,init}$ is the water outlet temperature when the solar radiation in interrupted, and T_i is the water inlet temperature
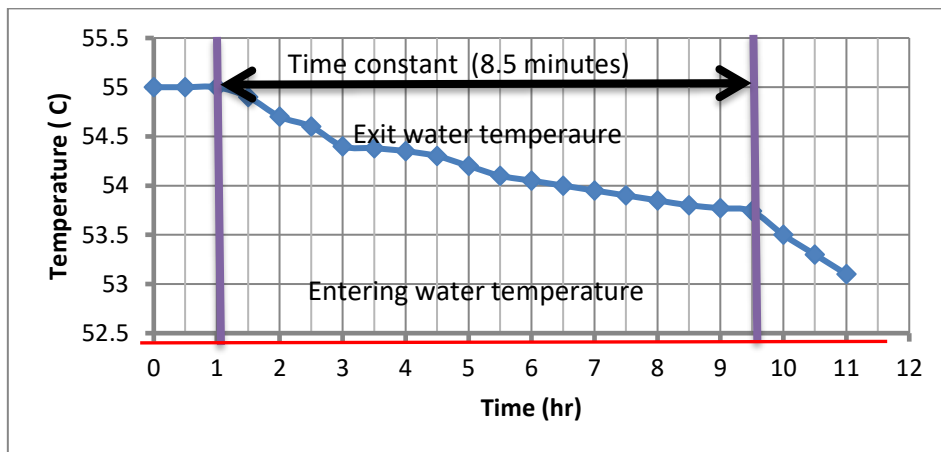
Figure 25. Time constant for 1500 LPH at 13:00 pm Jan. 2018.

It is found that the time constant for this test is 8.5 minutes. **Table 5** presented the heat removal factor which calculated analytically at 12:00 noon for each tests days by equation (10).

56

Table 5. Heat removal factor (F_R).

Volume flow rate (LPH)	F_R January 2018	F_R February 2018
500	0.65	0.54
750	0.78	0.69
1000	0.81	0.80
1250	0.72	0.83
1500	0.88	0.90

Fig. 26 Show the average collector efficiency that evaluated along the hourly day time and the heat removal factor. It be seen that the collector efficiency increase with increasing of the heat removal factor and decrease when the heat removal factor is reduced due to the improvement in the heat removal factor lead to increasing of useful heat. .
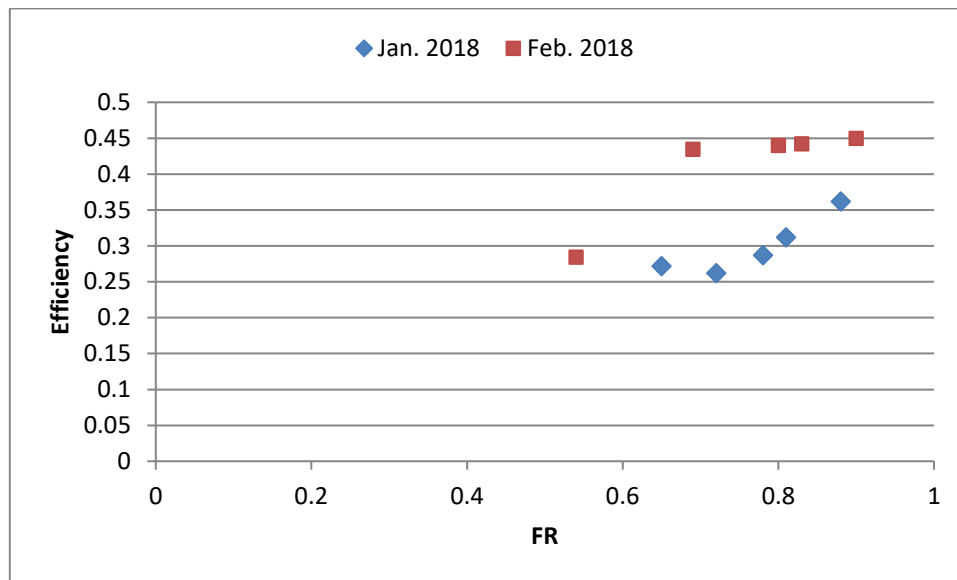
Figure 26. Thermal efficiency with FR.

8. CONCLUSIONS

The performance of plastic tube using as absorber inside flat plate solar collector for water heating was studied numerically and experimentally for outdoor conditions The experimental setup was done in Iraq- Babylon, that placed at 43.8^0 East longitude and $32^03'$ North latitude with titled of 45^0. The tests occurred outdoor on January and February 2018. The successful experiments were 10 for clear days. This work produced several conclusions as: The contour of absorber lead to improvement for thermal performance, The maximum output-input temperature difference was (3.1° C) occurs at (12:30 pm) for water volume flow rate of 1250 LPH on February2018, the

maximum collector thermal efficiency is 79% occurs at (12:30 pm) for water volume flow rate of 1250 LPH on February2018, and the maximum water storage temperature is 67 °C occurs at (16:00 pm) for water volume flow rate of 1250 LPH on February2018. The plastic tube can be used as absorber in winter reason.

9.REFERENCES

- Abdullah A.S., and Bassiouny M.K., 2014, Performance *of cylindrical plastic solar collectors for air heating*, Energy Conversion and Management, Vol. 88, pp. 88–95.

- Al-Douri Y., and Fayadh M. Abed, 2016, *Solar energy status in Iraq: Abundant or not—Steps forward*, Journal of Renewable and Sustainable Energy, Vol. 8 No. 2.

- Assilzadeha F., Kalogiroub S.A., Alia A., Sopiana K., 2005, *Simulation and optimization of a LiBr solar absorption cooling system with evacuated tube collector*, Renewable Energy, Vol. 30, PP. 1143–1159.

- Bansal N. K., Boeitcher A. and Uhlemann R., 1983, *Performance of Plastic Solar air Heating Collector with a Porous Absorber*, Energy Research, Vol. 7, PP. 375-384.

- Bartelsen B., Rockendorf G., V ennemann N., Tepe R., Lorenz K. and P urkarthofer G., 1999, *Elastomer-metal-absorber: Development and application*, Solar Energy, Vol. 67, No. 4-6, PP. 215-226.

- Bhaskaran Rajesh "Introduction to CFD Basics". 2013.

- Bird R. B., Armstrong R. C, and Hassager O., 1987, *Dynamics of Polymeric Fluids*, Fluid Mechanics, Vol. 1, Wiley: NY.

- Bridle R., Kiston L, and Wooders P., 2014, *Fossil-Fuel Subsidies: A barrier to renewable energy in five Middle East and North African countries*, Published by the International Institute for Sustainable Development.

- Brunold S. Entwicklung, and Kunststoffkollektoren, May 2010, *Grundlegende Fragestellungen und Ergebnisse eines Forschungsprojektes. In: 20. Symposium Thermische Solarenergie, Bad Staffelstein (DE)*, Regensburg: Ostbayerisches Technologie-Transfer-Institut, Vol. (OTTI), PP. 162-167.

- Christoph Nikolaus Reiter, 2014, *Polymeric Solar-Thermal Flat-Plate Collectors*, A thesis submitted in partial fulfilment of the requirements of De Montfort University for the degree of Doctor of Philosophy (PhD).

- Duffie J. A., and William A. Beckman, 2013, *Solar Engineering of Thermal Processes*, 4th edition, Wiley.

- Jacobson, E., Ketjoy, N., Nathakaranakule, S., and Rakwichian, W., 2006, *Solar parabolic trough simulation and application for a hybrid power plant in Thailand*, Vol. 32, No. 2, PP. 187-199.

- Kadhim Fadhil Nasir, 2017, *Experimental and Numerical Investigation on the performance characteristics of Flat Coil tube Water Solar Collector*, Journal of Babylon University/Engineering Science, Vol. 25, No. 4. PP. 1312-1327.

- Kaiser A., Fink C., Hausner R., and Ramschak T., 2012, *Leistungsanforderungen an Polymermaterialien in solarthermischen Systemen,* In: Gleisdorf Solar. Internationale Konferenz für thermische Solarenergienutzung,Gleisdorf (AT), September. Gleisdorf: AEE INTEC, pp. 296-306.

- Kalogirou Soteris A., 2004, *Solar thermal collectors and applications*, Progress in Energy and Combustion Science, Vol. 30, PP. 231–295.

- Li M., and Wang L. L., 2006, *Investigation of Evacuated Tube Heated by Solar Trough concentrating system*, Energy Conversion and Management, Vol. 47, PP. 3591–3601.

- Luis E. Juanicó, and Nicolás Di Lalla, 2013, *A New Low-Cost Plastic Solar Collector*, Hindawi Publishing Corporation ISRN Renewable Energy.

- Ma J., Sun W., Ji J., Zhang Y. , Zhang A., and Fan W., 2011, *Experimental and theoretical study of the efficiency of a dual function solar collector*, Applied Thermal Engineering, Vol. 31, PP.1751–1756.

- Mason A A, and Davidson J H., 1995, *Measured performance and modeling of an evacuated-tube, integral-collector-storage solar water heater*, J Sol Energy Eng. Vol. 117, No. 3, PP. 221–228.

- Pati P. P., and Dr. Deshmukh D.S., 2015, *Design Considerations for Flat Plate Solar Water Heater System*, Inernational Jouranal of Science, Spirituality business and Technology, Vol. 3, No. 2, PP. 2277—7261.

- Ramelan A H, Burhanuddin A, Fuady M I A, Wahyuningsih S, and Munawaroh H., 2016, *Flat Plate Solar Collector Characteristic with Shutter Glass Distance Variation and Collector Inclination Angle*, International Conference on Green and Renewable Energy Resources (ICGRER).

- Schmidt C, and Goetzberger A., 1990, *Single-tube integrated collector storage systems with transparent insulation and involute reflector*, Sol Energy, Vol. 45, No. 2, PP. 93–100.

- Schweiger, H., 1997, *Optimization of solar thermal absorber elements with transparent insulation*, PhD Thesis, Universitat Politècnica de Catalunya.

NOMENCLATURE

A   Area m^2

Ag   Area of glass cover m^2

Ar   Area of the receiver m^2

C_p Specific heat   J/kg.k

Dg   Cover effective length.   m

d   Diameter of the tube   m

F   Collector efficiency factor

F_R Heat removal factor

fc   Friction Factor

h   Heat transfer coefficient $W/m^2\ K$

h-(c.g-a)   convection heat transfer coefficient between ambient air and glass $W/\ m^2\ K$

h-(r,g-a)   Radiation heat transfer coefficient between glass cover and the ambient $W/m^2\ K$

h-(r,r-g)   Radiation heat transfer coefficient between receiver tube and glass cover. $W/m^2\ K$

hw   wind heat transfer coefficient $W/m^2\ K$

I   Incident of solar radiation $W/\ m^2$

K   Thermal conductivity   W/m K

K-ε   K-epsilon turbulence equations model

L   Tube length   m
m   Mass flow rate   kg/s
Nu   Nusselt number
Q   Heat transfer rate   W
Q_u energy added of collector   W
Re   Reynolds Number
t   time   s
T   Temperature   °C
U_L Overall heat loss coefficient   W/m^2 K
Uo   Overall heat transfer coefficient   W/m^2 K
V   velocity   m/s
v_r, v_θ, v_z velocity   m/s
Greek symbols
η Efficiency of collector
μ Dynamic viscosity   Kg/m.s
ρ Density   kg/m^3
ε Emissivity, turbulent kinematic energy dissipation rate
δ   constant

Subscripts
a   air, ambient, aperture
f   fluid
g   glass
i   Inlet
o   Outlet
r   radius, receiver
$r-\theta-z$ Cylindrical-polar coordinates
st   storage
th   thermal
w   wind, water